J|A|C|S
ARTICLES

Published on Web 10/29/2010

What Determines the Inhibition Effectiveness of ATA, BTAH, and BTAOH Corrosion Inhibitors on Copper?

Anton Kokalj,* Sebastijan Peljhan, Matjaž Finšgar, and Ingrid Milošev

Department of Physical and Organic Chemistry, Jozef Stefan Institute, Jamova 39, SI-1000 Ljubljana, Slovenia

Received August 26, 2010; E-mail: tone.kokalj@ijs.si

Abstract: Three corrosion inhibitors for copper—3-amino-1,2,4-triazole (ATA), benzotriazole (BTAH), and 1-hydroxybenzotriazole (BTAOH)—were investigated by corrosion experiments and atomistic computer simulations. The trend of corrosion inhibition effectiveness of the three inhibitors on copper in near-neutral chloride solution is determined experimentally as BTAH $\gtrsim$ ATA $\gg$ BTAOH. A careful analysis of the results of computer simulations based on density functional theory allowed to pinpoint the superior inhibiting action of BTAH and ATA as a result of their ability to form strong N−Cu chemical bonds in deprotonated form. While these bonds are not as strong as the Cl−Cu bonds, the presence of solvent favors the adsorption of inhibitor molecules onto the surface due to stronger solvation of the Cl^- anions. Moreover, benzotriazole displays the largest affinity among the three inhibitors to form intermolecular aggregates, such as $[BTA-Cu]_n$ polymeric complex. This is another factor contributing to the stability of the protective inhibitor film on the surface, thus making benzotriazole an outstanding corrosion inhibitor for copper. These findings cannot be anticipated on the basis of inhibitors' molecular electronic properties alone, thus emphasizing the importance of a rigorous modeling of the interactions between the components of the corrosion system in corrosion inhibition studies.

1. Introduction

Corrosion plays a very important role in diverse fields of industry and, consequently, in the economy. The protection of metals and alloys is therefore of paramount importance. The goal of studying corrosion processes is to find means of minimizing corrosion or preventing it from occurring. One way to protect from corrosion is to use the corrosion inhibitors. A corrosion inhibitor is a substance used in a very small amount that effectively reduces the corrosion rate. Many efficient inhibitors are heterocyclic organic compounds consisting of a π-system and/or containing O, N, or S heteroatoms.[1−3]

The mechanism of how organic corrosion inhibitors work is usually not known. It is, however, generally accepted that, in the majority of cases, the inhibition of corrosion is achieved through the interaction between corrosion inhibitor molecules and the metal surface, thus resulting in the formation of an inhibitive surface film, yet neither the mechanism of formation nor the atomic structure of such films is usually resolved.[1−3] Therefore, in most cases, good corrosion inhibitors were determined in a purely empirical manner out of large sets of organic compounds, where experimental testing provided the information on whether a specific molecule is effective or not for a certain substrate in a given medium.[1,2]

Recently, the use of quantum chemical methods has become very fashionable for screening new potential corrosion inhibitors—e.g., see ref 4 and the references therein. In the majority of cases, such screening consists of calculating several electronic structure parameters of isolated molecules either in the gas phase or in the aqueous phase, with the solvent treated by the polarized continuum model. Although in many cases the correlation between molecular electronic structure parameters and inhibition effectiveness against corrosion has been established, such an approach provides little physical insight into the actual corrosion inhibition mechanism. Despite the apparent success of this approach, there are cases where either similar molecules display strikingly different inhibition effectiveness[5] or, for a given set of inhibitors, there is no *obvious* correlation between their established inhibition effectiveness and computed electronic parameters.[6,7] This calls for a more rigorous modeling of the corrosion inhibition phenomenon.

Therefore, in this paper we present an application of such a rigorous modeling of corrosion inhibition with explicit treatment of the inhibitor−surface interaction. The solvent and the electric field effects at the metal/water interface are also considered. In particular, we investigate benzotriazole (BTAH) and two other triazole derivatives, 1-hydroxybenzotriazole (BTAOH) and 3-amino-1,2,4-triazole (ATA), as copper corrosion inhibitors in near-neutral chloride solutions. The structures of the three molecules and the numbering of atoms are shown in Figure 1.

(1) Schmitt, G. *Br. Corros. J.* **1984**, *19*, 165–176.
(2) Antonijevic, M. M.; Petrovic, M. B. *Int. J. Electrochem. Sci.* **2008**, *3*, 1–28.
(3) Bockris, J. O.; Reddy, A. K. N. *Modern Electrochemistry*, 2nd ed.; Kluwer Academic/Plenum Publishers: New York/Boston/Dordrecht/London/Moscow, 2000; Vol. 2B.
(4) Gece, G. *Corros. Sci.* **2008**, *50*, 2981–2992.
(5) Finšgar, M.; Lesar, A.; Kokalj, A.; Milošev, I. *Electrochim. Acta* **2008**, *53*, 8287–8297.
(6) Li, W.; He, Q.; Pei, C.; Hou, B. *Electrochim. Acta* **2007**, *52*, 6386–6394.
(7) Khalil, N. *Electrochim. Acta* **2003**, *48*, 2635–2640.

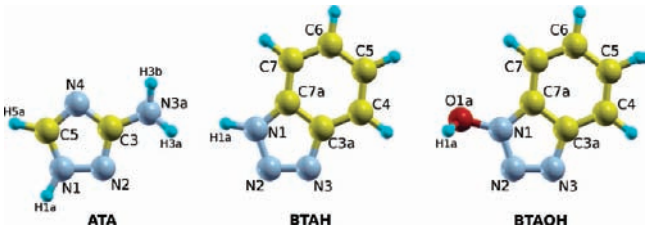

Figure 1. Optimized molecular structures of ATA, BTAH, and BTAOH and the numbering of the constituent atoms as used in this work.

BTAH is among the most effective copper corrosion inhibitors[2,8] and has attracted much attention since the pioneering work of Cotton and Scholes[9] and Poling.[10] The first application of BTAH was patented in 1947.[11] Since then, BTAH has been a subject of many patents (refs 12, 13, and references therein). As a corrosion inhibitor it is utilized in many different applications,[14−18] and its greatest use is to protect copper and its alloys under immersed conditions, but it can be also used as a vapor-phase corrosion inhibitor.[12,13] ATA is also an effective corrosion inhibitor for copper.[19−22] On the other hand, the performance of BTAOH is substantially worse.[5,23]

The choice to study ATA, BTAH, and BTAOH corrosion inhibitors was made not only because ATA and BTAH are very effective corrosion inhibitors for copper, but even more so due to the fact that, on the basis of molecular electronic parameters alone,[5,24] one would anticipate a trend of corrosion inhibition effectiveness that is incompatible with experiment. This deficiency makes the study suitable for gaining new physical insight into the actual inhibition mechanism. We build on our previous study, where we preliminarily described the gas-phase adsorption of individual inhibitor molecules on Cu(111).[25]

We first unambiguously determine the trend of corrosion inhibition effectiveness of the ATA, BTAH, and BTAOH inhibitors in near-neutral chloride solution by means of electrochemical and topography experiments, performed to consolidate the findings of previous studies.[5,26−28] We then present and carefully analyze the results of extensive computer simulations based on density functional theory (DFT) in order to scrutinize the corrosion inhibition mechanism and to provide an explanation for the observed trend of inhibition effectiveness. This was possible only by considering several involved phenomena, because the outcome depends on the interplay between them and cannot be explained by a single property or phenomenon.

2. Technical Details

Technical details and the method introduced to describe adsorption at the electrified surface are thoroughly described in the Supporting Information, while here only the most important points are presented.

Experimental Section. ATA, BTAH, and BTAOH were dissolved in 3% (w/w) aqueous NaCl. Solutions with 0.1, 1, and 10 mM concentration of each corrosion inhibitor were prepared. The corrosion inhibition effectiveness of inhibitors for copper was determined electrochemically by polarization resistance measurements. The performance of the inhibitors was also evaluated by topography measurements on the copper specimens, which were immersed for 30 days into stagnant 3% NaCl solutions containing either ATA, BTAH, or BTAOH. These measurements were performed on three different places on the 1 mm^2 spot size using a profilometer with vertical resolution of about 5 nm.

Computational Details. The adsorption of corrosion inhibitors was modeled on the slab model of a Cu(111) surface in the framework of DFT using the Perdew−Burke−Ernzerhof (PBE) energy functional[29] and the pseudopotential method with ultrasoft pseudopotentials[30,31] as implemented in the PWscf code from the Quantum ESPRESSO distribution.[32] As the PBE energy functional cannot describe the van der Waals interactions, the physisorption mode of adsorption was modeled using a reparameterized version[25] of the semiempirical correction of Grimme[33,34] (labeled as PBE-D). Electron affinities and solvation effects were calculated using the Gaussian03 program,[35] the local Gaussian-type orbital basis set 6-311++G(d,p) for H, C, N, and O atoms, and the modified all-electron TZVP basis set of Ahlrichs[36] for Cu atoms with the outer s, p, and d exponents reoptimized for Cu(111).[5] Aqueous solvent was described implicitly by the self-consistent reaction field theory based on Tomasi's polarized continuum model (PCM).[37−39] Molecular graphics were produced by the XCRYSDEN[40] graphical package.

Definitions. The following terms are defined to designate inhibitor molecules in specific forms: MolH, neutral form of the molecule (ATA, BTAH, BTAOH); Mol^-, deprotonated molecule

(8) Finšgar, M.; Milošev, I. *Corros. Sci.* **2010**, *52*, 2737–2749.
(9) Cotton, J. B.; Scholes, I. R. *Br. Corros. J.* **1967**, *2*, 1–5.
(10) Poling, G. W. *Corros. Sci.* **1970**, *10*, 359–37.
(11) Procter and Gamble, Ltd. British Patent 652339, 1947.
(12) Walker, R. *Anti-Corros. Methods Mater.* **1970**, *17*, 9–15.
(13) Walker, R. *Corrosion* **1973**, *29*, 290–296.
(14) Walker, R. *J. Chem. Educ.* **1980**, *57*, 789–791.
(15) Brinch Madsen, H. *Stud. Conserv.* **1967**, *12*, 163–167.
(16) Brinch Madsen, H. *Stud. Conserv.* **1971**, *16*, 120–122.
(17) Kim, J. J.; Kim, S.-K.; Bae, J. U. *Thin Solid Films* **2002**, *415*, 100–107.
(18) Cotton, J. B. Control of Surface Reactions on Copper by Means of Organic Reagents. In *Proceedings of the 2nd International Congress on Metallic Corrosion*; NACE: New York, 1963.
(19) Qafsaoui, W.; Blanc, C.; Pebere, N.; Srhiri, A.; Mankowski, G. *J. Appl. Electrochem.* **2000**, *30*, 959–966.
(20) Kuznetsov, Y. I.; Kazansky, L. P. *Russ. Chem. Rev.* **2008**, *77*, 219–232.
(21) Sherif, E.-S. M.; Erasmus, R. M.; Comins, J. D. *J. Colloid Interface Sci.* **2007**, *309*, 470–477.
(22) Sherif, E.-S. M.; Erasmus, R. M.; Comins, J. D. *J. Colloid Interface Sci.* **2007**, *311*, 144–151.
(23) Finšgar, M.; Milošev, I. *Mater. Corros.* **2010**; doi: 10.1002/maco.201005645.
(24) Kokalj, A. *Electrochim. Acta* **2010**; doi: 10.1016/j.electacta.2010.09.065.
(25) Kokalj, A.; Peljhan, S. *Langmuir* **2010**, *26*, 14582–14593.
(26) Finšgar, M.; Milošev, I.; Pihlar, B. *Acta. Chim. Slov.* **2007**, *54*, 591–597.
(27) Fleischmann, M.; Hill, I. R.; Mengoli, G.; Musiani, M. M.; Akhavan, J. *Electrochim. Acta* **1985**, *30*, 879–888.
(28) Moretti, G.; Molokanov, V. V.; Quartarone, G.; Zingales, A. *Corrosion* **1998**, *54*, 135–144.
(29) Perdew, J. P.; Burke, K.; Ernzerhof, M. *Phys. Rev. Lett.* **1996**, *77*, 3865–3868.
(30) Vanderbilt, D. *Phys. Rev. B* **1990**, *41*, 7892–7895.
(31) Ultrasoft pseudopotentials (US PP) for H, C, N, O, and Cu were taken from the Quantum Espresso PseudoPotential Download Page, http://www.quantum-espresso.org/pseudo.php (files: H.pbe-rrkjus.UPF, C.pbe-rrkjus.UPF, N.pbe-rrkjus.UPF, O.pbe-rrkjus.UPF, and Cu.pbe-d-rrkjus.UPF).
(32) Giannozzi, P.; et al. *J. Phys.: Cond. Matter.* **2009**, *21*, 395502.
(33) Grimme, S. *J. Comput. Chem.* **2006**, *27*, 1787–1799.
(34) Barone, V.; Casarin, M.; Forrer, D.; Pavone, M.; Sambi, M.; Vittadini, A. *J. Comput. Chem.* **2009**, *130*, 934–939.
(35) Frisch, M. J.; et al. *Gaussian 03*, Revision C.02; Gaussian, Inc.: Wallingford CT, 2004.
(36) Schäfer, A.; Huber, C.; Ahlrichs, R. *J. Chem. Phys.* **1994**, *100*, 5829–5835.
(37) Cancès, E.; Mennucci, B.; Tomasi, J. *J. Chem. Phys.* **1997**, *107*, 3032–3041.
(38) Mennucci, B.; Cances, E.; Tomasi, J. *J. Phys. Chem. B* **1997**, *101*, 10506–10517.
(39) Tomasi, J.; Mennucci, B.; Cammi, R. *Chem. Rev.* **2005**, *105*, 2999–3094.
(40) Kokalj, A. *Comput. Mater. Sci.* **2003**, *28*, 155–168. Code available from http://www.xcrysden.org/.

with the proton H1a$^+$ removed (ATA$^-$, BTA$^-$, BTAO$^-$); Mol$^\odot$, dehydrogenated molecular radical without the H1a hydrogen (ATA$^\odot$, BTA$^\odot$, BTAO$^\odot$; the $\odot$ symbol is used to indicate radical species and their properties); Mol(H), either Mol or MolH.

Adsorption geometries are designated as *site-atomlist*, where *site* designates the site on the surface to which the molecule bonds with the atoms specified by *atomlist*. For example, designation bridge-N2,N3 specifies the molecule adsorbed over the bridge site with N2 and N3 atoms attached to the surface.

2.1. Evaluation of Adsorption Energies. The adsorption of inhibitor molecules in neutral and deprotonated forms is considered because the pK_a values at 25 °C — referring to the reaction MolH $\rightleftharpoons$ H$^+$ + Mol$^-$ — are 10.5,[41] 8.38,[42] and 4.46[43] for ATA, BTAH, and BTAOH, respectively. Hence, at pH = 7, ATA and BTAOH are almost exclusively in neutral and deprotonated forms, respectively, whereas BTAH is present in both forms, with the neutral/deprotonated ratio of about 96/4. Moreover, the molecules may also deprotonate on the surface, because it has been recently demonstrated that under-coordinated defects on copper surfaces are reactive enough to dehydrogenate unsaturated organic molecules.[44]

The convention that exothermic energies are negative is used throughout.

Adsorption from Gas Phase. As for the adsorption of deprotonated molecules, we avoid using the charged species for the calculations employing periodic boundary conditions. The gas-phase adsorption energy, calculated with respect to Mol$^-$ in the initial state, is therefore calculated using the following thermodynamic cycle:

$$\begin{array}{lcll} \mathrm{Mol}^-_{(g)} & \rightarrow & \mathrm{Mol}^\odot_{(g)} + 1e^- & \Delta E = E^\odot_{ea} \\ 1e^- + \mathrm{metal} & \rightarrow & \mathrm{metal}^- & \Delta E = -\Phi \\ \mathrm{Mol}^\odot_{(g)} & \rightarrow & \mathrm{Mol}^\odot_{(ad)} & \Delta E = E^\odot_{ads} \end{array} \quad (1)$$

where $E^\odot_{ea}$ is the electron affinity of the Mol$^\odot$ radical and $E^\odot_{ads}$ its adsorption (binding) energy, while Φ is the work function of the metal surface; for Cu(111) the calculated value is 4.68 eV.[45] The adiabatic $E^\odot_{ea}$ was calculated as $E^\odot_{ea} = E_{\mathrm{Mol}^\odot} - E_{\mathrm{Mol}^-}$ by using the local 6-311++G(d,p) Gaussian-type-orbital basis set. The $E^\ominus_{ads}$ is therefore

$$E^\ominus_{ads} = E^\odot_{ads} + E^\odot_{ea} - \Phi \quad (2)$$

This equation holds in the limit of very low coverage due to the use of the work function of clean Cu(111). For higher coverages, the adsorption-induced work function change should be taken into account. The $E^\odot_{ads}$ is taken as a more appropriate measure of the Mol−Cu(111) bond strength than the $E^\ominus_{ads}$, because the latter contains also the gain in energy as the electron passes from Mol$^-$ to the metal surface.

Adsorption from Aqueous Phase. On changing from gas to aqueous phase, the free energy G is used in favor of energy E, because G is the more appropriate thermodynamic potential in the liquid phase. This also helps in identifying in which phase a given contribution is calculated (E in the gas phase and G in the aqueous phase). The adsorption free energy for a deprotonated molecule at the water/solid interface is calculated by employing the following thermodynamic cycle:[46]

$$\begin{array}{ll} \mathrm{Mol}^-_{(aq)} \rightarrow \mathrm{Mol}^-_{(g)} & \Delta G = -\Delta G^{\mathrm{Mol}^-}_{solv} \\ \mathrm{Cu}(111)_{(aq)} \rightarrow \mathrm{Cu}(111)_{(g)} & \Delta G = -\Delta G^{\mathrm{Cu}(111)}_{solv} \\ \mathrm{Mol}^-_{(g)} \rightarrow \mathrm{Mol}^\odot_{(g)} + e^- & \Delta G = E^\odot_{ea} \\ \mathrm{Mol}^\odot_{(g)} + \mathrm{Cu}(111)_{(g)} \rightarrow \mathrm{Mol{-}Cu}(111)_{(g)} & \Delta G \approx E^\odot_{ads} \\ \mathrm{Mol{-}Cu}(111)_{(g)} \rightarrow \mathrm{Mol{-}Cu}(111)_{(aq)} & \Delta G = \Delta G^{\mathrm{Mol\text{-}Cu}(111)}_{solv} \\ \mathrm{Mol{-}Cu}(111)_{(aq)} + e^- \rightarrow \mathrm{Mol{-}Cu}(111)^-_{(aq)} & \Delta G = -\Phi^* \end{array} \quad (3)$$

where Φ^* is the work function of the metal/water/vacuum system, which also corresponds to an absolute electrode potential as defined by Trasatti;[47] for copper at the potential of zero charge (PZC), $\Phi^*_{pzc} = \Phi - 0.73$ eV.[47,48] ΔG_{solv} designates solvation free energies of individual components. It is convenient to define

$$\Delta\Delta G^{\mathrm{Mol//Cu}}_{solv} = \Delta G^{\mathrm{Mol\text{-}Cu}(111)}_{solv} - \Delta G^{\mathrm{Cu}(111)}_{solv} \quad (4)$$

Hence,

$$\Delta G^{\ominus(aq)}_{ads} = E^\odot_{ads} + E^\odot_{ea} - \Phi^* - \Delta G^{\mathrm{Mol}^-}_{solv} + \Delta\Delta G^{\mathrm{Mol//Cu}}_{solv} \quad (5)$$

The $\Delta\Delta G^{\mathrm{Mol(H)//Cu}}_{solv}$ is evaluated by a relatively large cluster models of the Mol(H)/Cu(111) system that is immersed into implicit solvent with the geometry kept fixed to that calculated at the metal/vacuum interface by the slab model.

Adsorption at Electrified Surface. To account for the applied electrode potential, the $\Delta G^{(aq)}_{ads}$ is written as a function of externally applied electric field, **E**, which for deprotonated molecules is given by

$$\Delta G^{\ominus(aq)}_{ads}(\mathbf{E}) = E^\odot_{ads}(\mathbf{E}) + E^\odot_{ea} - \Phi^*(\mathbf{E}) - \Delta G^{\mathrm{Mol}^-}_{solv} + \Delta\Delta G^{\mathrm{Mol//Cu}}_{solv}(\mathbf{E}) \quad (6)$$

The terms that do not depend on **E** are those corresponding to phenomena not taking place at the metal/solution interface. The $E^\odot_{ads}(\mathbf{E})$ is evaluated by performing structural relaxations at several predefined values of **E**. The $\Phi^*(\mathbf{E})$ is treated within the Helmholtz−Perrin parallel plate capacitor model of double layer; hence,

$$\Phi^*(\mathbf{E}) = \Phi^*_0 + ed\mathbf{nE} \quad (7)$$

where Φ^*_0 is a value at zero external field, e is the unit charge, **n** is the surface normal, and the proportionality constant d is the thickness of the double layer. By postulating its value, an approximate relation between the electric field **E** and electrode potential Φ^*/e is established. For illustrative purposes, we will use the value of $d = 3$ Å.[49]

The exact treatment of $\Delta\Delta G^{\mathrm{Mol//Cu}}_{solv}(\mathbf{E})$ is very difficult; therefore, this term is evaluated approximately by considering the behavior of the water bilayer on Cu(111) as a function of electric field (see Supporting Information for more details).

For a neutral molecule, the expression for $\Delta G^{(aq)}_{ads}$ is

$$\Delta G^{(aq)}_{ads}(\mathbf{E}) = E_{ads}(\mathbf{E}) - \Delta G^{\mathrm{MolH}}_{solv} + \Delta\Delta G^{\mathrm{MolH//Cu}}_{solv}(\mathbf{E}) \quad (8)$$

3. Experimental Determination of the ATA, BTAH, and BTAOH Inhibiting Action

To establish the trend in corrosion inhibition effectiveness of ATA, BTAH, and BTAOH in near-neutral chloride solutions,

(41) Pichon, V.; Hennion, M.-C. *Anal. Chim. Acta* **1993**, *284*, 317–326.
(42) Hansen, L. D.; West, B. D.; Baca, E. J.; Blank, C. L. *J. Am. Chem. Soc.* **1968**, *90*, 6588–6592.
(43) Hammud, H. H.; Holman, K. T.; Masoud, M. S.; El-Faham, A.; Beidas, H. *Inorg. Chim. Acta* **2009**, *362*, 3526–3540.
(44) Kravchuk, T.; Vattuone, L.; Burkholder, L.; Tysoe, W. T.; Rocca, M. *J. Am. Chem. Soc.* **2008**, *130*, 12552–12553.
(45) Peljhan, S.; Kokalj, A. *J. Phys. Chem. C* **2009**, *113*, 14363–14376.
(46) Koper, M. T. M.; van Santen, R. A. *Surf. Sci.* **1999**, *422*, 118–131.
(47) Trasatti, S. *Electrochim. Acta* **1991**, *36*, 1659–1667.
(48) Heras, J. M.; Viscido, L. *Appl. Surf. Sci.* **1980**, *4*, 238–241.
(49) The value of 3 Å is frequently used for the thickness of the double layer.[92−94] This value is used for all the cases considered, although organic adsorbates increase the thickness of the double layer[95] (note that we consider the limit of very small coverage).

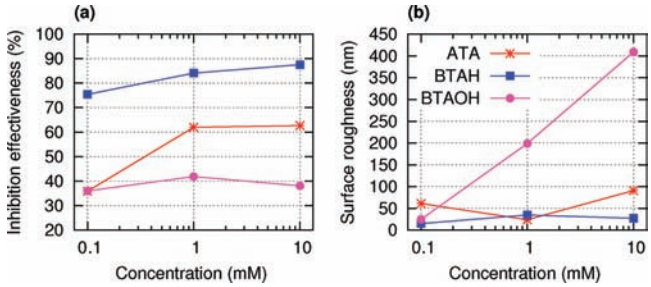

Figure 2. Performance of ATA, BTAH, or BTAOH corrosion inhibitors for copper in 3% NaCl as a function of their concentrations: (a) inhibition effectiveness and (b) average mean surface roughness of inhibited Cu specimens after being exposed for 30 days in 3% NaCl solution.

we analyzed their inhibiting action by means of polarization resistance (R_p) measurements and by a set of comparative topography measurements. The premise behind the R_p measurements is that, in the presence of corrosion inhibitor, the R_p value increases because of an increased resistance of the metal to transfer of electrons to electroactive species in solution, which is due to the formation of a protective layer. On the other hand, the use of topography is based on the argument that corrosion inhibitors protect the metal surface and reduce its roughening. The predominant types of corrosion in chloride solutions are pitting and uniform (general) corrosion,[50,51] which both contribute to the increased surface roughness.[5]

In each inhibitor-containing solution, an increase in the polarization resistance was observed compared to the uninhibited solution, indicating the corrosion inhibition characteristics of ATA, BTAH, and BTAOH. The resulting inhibition effectiveness, IE, defined by eq S1 in the Supporting Information, as a function of the corrosion inhibitor concentration is shown in Figure 2a. The IE of BTAOH is about 40% throughout, whereas the IE of ATA is about 40% at 0.1 mM concentration and increases to about 60% for concentrations $\geq$1 mM. BTAH shows the largest IE values and an increasing IE dependence on the concentration. The IE reaches almost 90% at 10 mM concentration.

Additional information about the corrosion inhibition performance of the three inhibitors is provided by topography measurements of copper specimens that corroded under realistic conditions. The calculated average values of mean surface roughness, S_a, defined by eq S2 in the Supporting Information, are shown in Figure 2b as a function of concentration, whereas 3D representations of surface profiles are shown in Figure 3. The average S_a value of the Cu specimens after the grinding and polishing procedure was 18 nm. When the specimens were exposed for 30 days in inhibited 3% NaCl solution, differences between the three inhibitors appeared, particularly so at higher concentrations, as evidenced by Figures 2b and 3. Average S_a values for the three inhibitors were the closest at 0.1 mM concentration, S_a being 61, 15, and 25 nm for ATA, BTAH, and BTAOH, respectively. Note that, in the case of 0.1 mM BTAOH, the Cu surface was covered by a dark but very smooth layer of corrosion products (presumably CuO) as a consequence of extensive uniform corrosion. For this reason, the corresponding 3D profile in Figure 3 is colored brownish, even though the surface was not very rough. No such discoloration of surfaces was observed for BTAH and ATA. At higher concentrations, the differences between inhibitors are bigger. Average S_a values of Cu specimens exposed to 1 and 10 mM BTAOH are 199 and 409 nm, respectively, and are therefore significantly larger than at 0.1 mM concentration, indicating that BTAOH at higher concentrations is not suitable as a Cu corrosion inhibitor in 3% NaCl stagnant solution. On the other hand, at 1 and 10 mM concentrations of either BTAH or ATA, S_a value remains low. Only at 10 mM ATA does it increase a bit, reaching an average S_a value of 91 nm. These results indicate that, while BTAH and ATA substantially reduce the rate of corrosion, BTAOH does not.

The yellow islands visible on specimens immersed in 1 mM BTAH and 10 mM ATA solutions (Figure 3) were analyzed by using a scanning electron microscope (SEM) equipped with energy dispersive X-ray spectroscopy (EDXS). As only Cu and O atoms were detected, and a significantly higher amount of O was found on the islands compared to smooth spots on the surface, we conclude that these islands are composed of copper oxides (results not shown).

Pitting corrosion was evaluated by the average number of pits equal to or deeper than 0.25 μm on three different 1 mm^2 spots (Table 1). A large number of pits was found in the case of 1 and 10 mM concentrations of BTAOH due to very rough surfaces, where pits were all over the surface (Figure 3). No pitting was observed at any BTAH concentration, in agreement with previous observations,[52] and few pits were found in the case of 0.1 and 10 mM concentrations of ATA. The extent of pitting corrosion therefore increases in the order of BTAH $\lesssim$ ATA $\ll$ BTAOH.

On the basis of the results presented above, we conclude that BTAH is the most effective corrosion inhibitor for copper in near-neutral chloride solutions. ATA has similar corrosion inhibition characteristics, although it shows a somewhat lower inhibition effect for pitting corrosion. On the other hand, BTAOH performs much worse against both pitting and general type of corrosion. The corrosion inhibition performance of the three inhibitors therefore follows the trend BTAH $\gtrsim$ ATA $\gg$ BTAOH. These findings are in line with previous studies, where it has been shown, under compatible experimental conditions, that BTAH is better than ATA,[26] and BTAH is better than BTAOH.[5,23] A slightly different finding was reported under more alkaline conditions (pH = 9) of prepassivated copper in borate-buffered solution containing 0.2 M chloride, where ATA outperformed BTAH for pitting corrosion, whereas BTAH was better for preventing uniform corrosion.[19]

4. Adsorption at Cu(111)/Vacuum Interface

To aid in explaining the experimentally determined trend of corrosion inhibition effectiveness, we modeled the interaction of inhibitors with the copper surface, where Cu(111) was chosen as representative because it is the most stable low Miller index copper surface[53] and hence the most abundant.

4.1. Adsorption of Individual Molecules. In this subsection we build on our previous study,[25] where the adsorption of individual stand-alone molecules in neutral and deprotonated forms on Cu(111) was studied. We start by summarizing the main adsorption characteristics to facilitate comprehension of

(50) Finšgar, M.; Fassbender, S.; Hirth, S.; Milošev, I. *Mater. Chem. Phys.* **2009**, *116*, 198–206.
(51) Finšgar, M.; Fassbender, S.; Nicolini, F.; Milošev, I. *Corros. Sci.* **2009**, *51*, 525–533.
(52) Cruickshank, B. J.; Gewirth, A. A.; Rynders, R. M.; Alkire, R. C. *J. Electrochem. Soc.* **1992**, *139*, 2829–2832.
(53) Vitos, L.; Ruban, A. V.; Skriver, H. L.; Kollár, J. *Surf. Sci.* **1998**, *411*, 186–202.

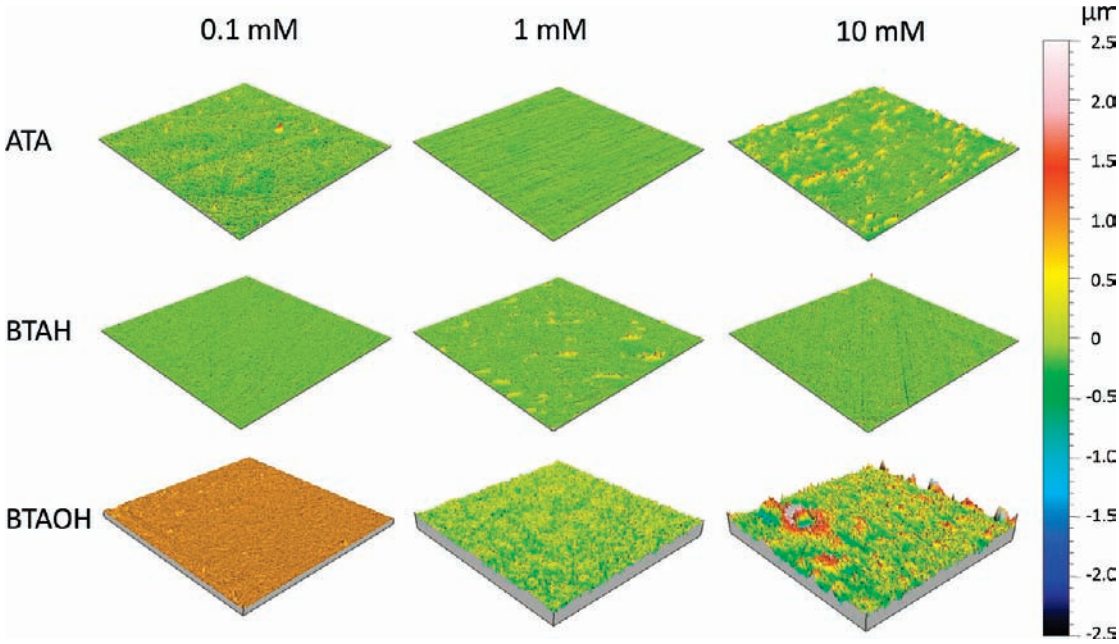

Figure 3. Topography profiles obtained by a profilometer. The coloring is according to the scale shown on the right, which spans ±2.5 μm range, except for the profile of 0.1 mM BTAOH, which is colored brownish to indicate the formation of a dark corrosion product (see text).

Table 1. Average Number of Pits Equal to or Deeper than 0.25 μm on Three Different 1 mm^2 Spots

	inhibitor concentration		
	0.1 mM	1 mM	10 mM
ATA	4	0	9
BTAH	0	0	0
BTAOH	12	2638	2625

the subject. Both chemisorption and physisorption modes of adsorption are considered; the two terms are used to designate the type of molecule−surface interaction and not the scale of the interaction energy. Chemisorption is characterized by formation of molecule−surface chemical bonds, whereas physisorption is driven by van der Waals dispersion forces. For chemisorption, the molecule−surface distances are about 2 Å, as inferred from the covalent radii, $r^{N}_{cov} + r^{Cu}_{cov} = 1.28 + 0.75 =$ 2.03 Å, whereas for physisorption they are substantially longer, about 3 Å (sum of the van der Waals radii is $r^{N}_{vdw} + r^{Cu}_{vdw} =$ 1.55 + 1.40 = 2.95 Å).

4.1.1. Chemisorption. Neutral molecules chemisorb weakly to the surface. The strength of the chemisorption increases in the order BTAH < BTAOH < ATA, with adsorption energies of −0.40, −0.53, and −0.60 eV, respectively. The molecules bond to the surface with triazole nitrogen atoms and also through X−H···metal hydrogen bonds[25] (X = N or O), as seen in Figure 4. The N−Cu bond lengths are similar for the three molecules, being about 2.1 Å, as anticipated above for the chemisorption, whereas the H···metal bond lengths range from 2.3 to 2.7 Å. The ATA binds to the top site with the N2 atom—designated as top-N2 adsorption mode—and in addition forms two N−H···metal hydrogen bonds with the H1a and H3a atoms. The BTAH also adsorbs in the top-N2 mode and forms one N−H···metal hydrogen bond with the Ha1 atom. In addition, BTAH can also adsorb in the bridge-N2,N3 mode without forming an X−H···metal hydrogen bond. This site is only slightly less stable than the top-N2. The BTAOH adsorbs in the bridge-N2,N3 mode and forms one O−H···metal hydrogen bond with the H1a atom.

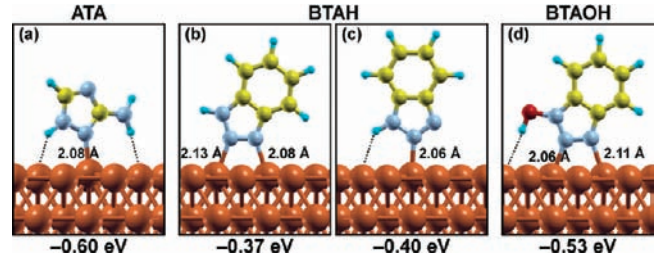

Figure 4. The most stable optimized structures of ATA, BTAH, and BTAOH chemisorbed on Cu(111). The number below each plot is the corresponding chemisorption energy.

Molecule−surface bonding is substantially enhanced near the under-coordinated defects, in accord with previous adsorption studies on unsaturated organic molecules.[54,55] At the step edge defect consisting of a (111) terrace and a (111) step riser, the BTAH adsorption energy is −0.71 eV [compared to −0.40 eV on perfect Cu(111)].

Contrary to the adsorption of neutral molecules, deprotonated molecules chemisorb strongly to the surface. The strength of the chemisorption, as measured by $E^{\odot}_{ads}$, increases in the order $BTAO^{\odot} < ATA^{\odot} < BTA^{\odot}$, with the $E^{\odot}_{ads}$ adsorption energies of −1.65, −2.22, and −2.78 eV, respectively. As can be seen from Figure 5, deprotonated molecules chemisorb in an upright geometry with two neighboring triazole nitrogen atoms bonded to the surface. In addition, the $BTAO^{\odot}$ can also chemisorb via the O1a atom instead of the N3 atom (Figure 5d), in agreement with the proposition made by Graff et al. on the basis of surface-enhanced Raman scattering measurements.[56] This latter form is even slightly more stable than the bridge-N2,N3 form. Due to a much stronger bonding of deprotonated molecules to the

(54) Kokalj, A.; Dal Corso, A.; de Gironcoli, S.; Baroni, S. *J. Phys. Chem. B* **2002**, *106*, 9839–9846.
(55) Kokalj, A.; Dal Corso, A.; de Gironcoli, S.; Baroni, S. *Surf. Sci.* **2004**, *566−568*, 1018–1023.
(56) Graff, M.; Bukowska, J.; Zawada, K. *J. Electroanal. Chem.* **2004**, *567*, 297–303.

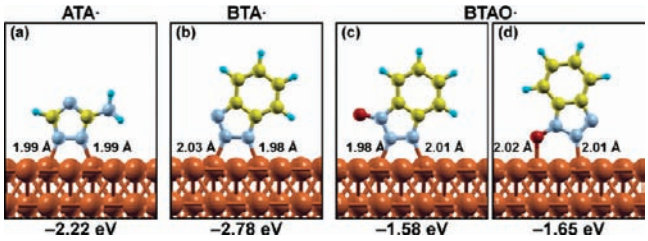

Figure 5. Optimized structures of deprotonated (dehydrogenated) (a) ATA$^{\odot}$, (b) BTA$^{\odot}$, and (c,d) BTAO$^{\odot}$ chemisorbed on Cu(111). The number below each plot is the corresponding $E_{ads}^{\odot}$ chemisorption energy.

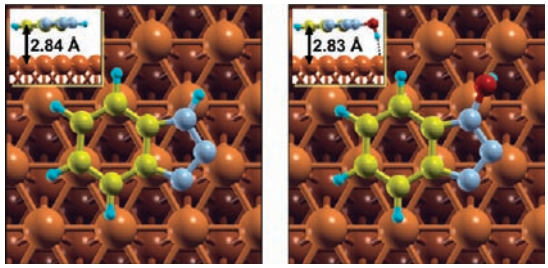

Figure 6. Optimized structures of BTAH and BTAOH physisorbed on Cu(111). The corresponding PBE-D calculated physisorption energies are −0.72 and −0.97 eV, respectively.

surface compared to the bonding of the neutral forms, the N−Cu distances are about 0.1 Å shorter for the former, thus being close to 2 Å.

4.1.2. Physisorption. Physisorption is treated with the PBE-D energy functional, because the PBE alone cannot describe the van der Waals interaction. The PBE-D calculated physisorption energy of ATA is −0.56 eV. However, this state is metastable: it is either a very shallow minimum or a flat plateau. On the other hand, the BTAH and BTAOH molecules physisorb rather strongly. At a low 1/16 monolayer (ML) coverage, the calculated E_{ads} values are −0.72 and −0.97 eV, respectively. The reason for the ∼0.25 eV more exothermic value for BTAOH is the formation of an O−H···metal hydrogen bond. The physisorption molecular geometries are nearly parallel to the surface (see Figure 6), with the benzene fragment being closer to the surface: the lower end of the molecule is ∼2.8 Å above the surface, whereas the upper part is at ∼3.1 Å.

The physisorption adsorption mode was not considered explicitly for deprotonated molecules because their chemisorption energies, $E_{ads}^{\odot} \in [-2,-3]$ eV, are far more exothermic than the physisorption energies of neutral molecular forms, $E_{ads} \approx -1$ eV, and the two forms are expected to display similar physisorption energies due to their very similar molecular sizes. All these indicate that deprotonated molecules strongly favor chemisorption.

4.2. Intermolecular Associations. It has been often assumed that the inhibition of corrosion is due to formation of a stable and protective surface film composed of corrosion inhibitor molecules, which blocks or hinders the reactive species from coming into close contact with the surface.[18,57,58] In this context, the intermolecular interactions may play an important role, because the formation of such a protective film is likely due to interplay between the molecule−surface and the lateral molecule−molecule interactions, which may involve also the formation of organometallic network complexes on the surface. For this reason, two modes of intermolecular association are considered below: intermolecular hydrogen-bonding and organometallic complex formation.

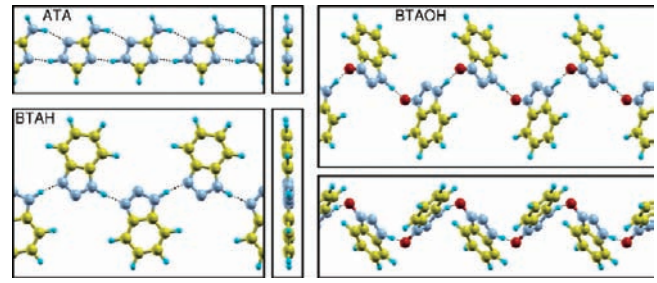

Figure 7. Structures of optimized periodic models of H-bonded polymers of ATA, BTAH, and BTAOH.

4.2.1. Intermolecular H-Bonding of Neutral Molecules. All three molecules studied here contain hydrogen linked either to nitrogen (BTAH and ATA) or to oxygen (BTAOH), which are electronegative enough to form intermolecular H-bonds. Indeed, these molecules and their derivatives are known to form a variety of H-bonded associations either in their crystal structures or in organometallic complexes.[43,59−63]

First we consider intermolecular H-bonding between the individual molecules in the absence of a copper surface. Several periodic models of linear ATA, BTAH, and BTAOH polymers were considered, and some of them were derived on the basis of inhibitors' crystal structures.[59,61] Only the most stable identified structure for each molecule is reported below. For BTAH and BTAOH, the unit cell consists of two alternating molecules, whereas for ATA, the most stable identified structure is made of a single molecule per unit cell. The corresponding optimized structures are shown in Figure 7. It is seen that ATA and BTAH form planar polymer structures, whereas BTAOH forms a nonplanar zigzag polymer structure due to the OH group, of which the H points out of the molecular plane (e.g., see Figure 1). Moreover, in the BTAOH polymer structure, the H1a proton is shifted from the O1a to the N3 atom, i.e., O−H···N → O···H−N. This can be explained by the acidic nature of the H1a proton (BTAOH has a low pK_a value). Apparently, the polymer structure itself provides a sufficiently *alkaline* environment.

The PBE results concerning the H-bond strengths are summarized in Table 2. In the polymer structure, there is one intermolecular H-bond per molecule for BTAH and BTAOH, whereas for ATA there are two H-bonds per molecule which are not equivalent, hence an average H-bond strength is reported in the table. Each ATA, BTAH, and BTAOH molecule within the polymer is stabilized by 0.61, 0.52, and 0.76 eV, respectively. These values are comparable in magnitude to adsorption energies, thus demonstrating the importance of the intermolecular hydrogen-bonding.

H-Bonded Structures on Cu(111). The planar structure of H-bonded ATA and BTAH polymers is suitable for parallel

(57) Dugdale, I.; Cotton, J. *Corros. Sci.* **1963**, *3*, 69–74.
(58) Sastri, V. *Corrosion Inhibitors: Principles and Applications*; John Wiley & Sons: Chichester, 2001.
(59) Escande, A.; Galigné, J. L.; Lapasset, J. *Acta Crystallogr. B* **1974**, *30*, 1490–1495.
(60) Krawczyk, S.; Gdaniec, M. *Acta Crystallogr. E* **2005**, *61*, o2967–o2969.
(61) Bosch, R.; Jung, G.; Winter, W. *Acta Crystallogr. C* **1983**, *39*, 1089–1092.
(62) Chen, S.; Shu, S.; Gao, S. *Inorg. Chim. Acta* **2009**, *362*, 3043–3048.
(63) Matulková, I.; Nemec, I.; Teubner, K.; Nemec, P.; Micka, Z. *J. Mol. Struct.* **2008**, *873*, 46–60.

Table 2. Energetic and Structural Data for H-Bonded ATA, BTAH, and BTAOH Polymers[a]

	$d_{H\cdots X}$ (Å)	$D_{H\cdots X}$ (eV)	$n_{H\cdots X}$ (molecule^{-1})	ΔE_{stab} (eV/molecule)
ATA	1.73, 2.01	0.31[b]	2	−0.61
BTAH	1.71	0.52	1	−0.52
BTAOH	1.56	0.76	1	−0.76

[a] $d_{H\cdots X}$, H···X bond distance; $D_{H\cdots X}$, H-bond strength; $n_{H\cdots X}$, number of H-bonds per molecule; and ΔE_{stab}, stabilization energy of molecule within the polymer, $\Delta E_{stab} = -n_{H\cdots X}D_{H\cdots X}$. [b] Average H-bond strength.

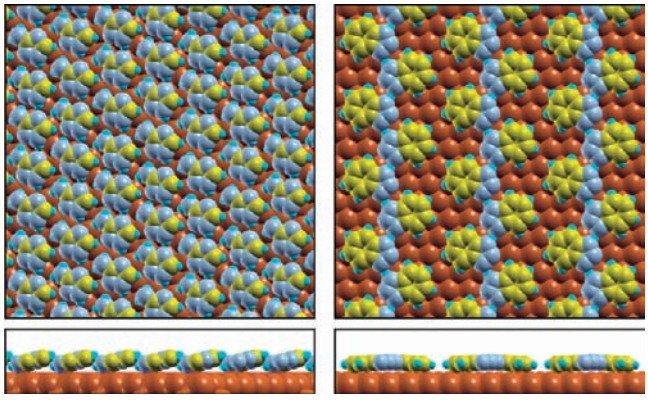

Figure 8. Top and side views of optimized intermolecular H-bonded networks of ATA (left) and BTAH (right) physisorbed on Cu(111). The corresponding PBE-D calculated physisorption (stabilization) energies are −1.12 and −1.23 eV/molecule, respectively.

modes of adsorption (physisorption); hence, the calculations were performed with the PBE-D functional. The resulting optimized structures on Cu(111) are shown in Figure 8, and the corresponding net adsorption energies are −1.12 and −1.23 eV/molecule for ATA and BTAH, respectively. These numbers are significantly more exothermic than the chemisorption or physisorption energies of the corresponding molecules alone. This large stabilization comes from the molecule−surface and lateral molecule−molecule interactions, and the two contributions are almost additive. For ATA, −0.56 eV (physisorption energy) and −0.61 eV (lateral H-bonding) sums to −1.17 eV; for BTAH, −0.72 eV (physisorption energy) and −0.52 eV (lateral H-bonding) sums to −1.24 eV.

The adsorption of H-bonded polymers was not considered for neutral BTAOH, because it exists in deprotonated form in near-neutral solutions due to its low pK_a value.

4.2.2. Intermolecular H-Bonding of Deprotonated Molecules. Fang et al.[64] proposed a structural model where deprotonated BTA^- molecules are interconnected with the C4−H···N1 hydrogen bonds (numbering of atoms according to Figure 1). This suggestion has been often criticized because it is believed the C−H cannot form H-bonds. Our calculations reveal that the C−H···N1 hydrogen bond is very weak; the calculated bond strength is merely 0.10 eV in the isolated H-bonded BTA dimer. We further find that such bonding is not feasible for adsorbed BTA molecules, in agreement with previous DFT calculations of Jiang and Adams.[65] The molecules in the geometry proposed by Fang repel and in the final optimized geometry are well separated.

A deprotonated ATA molecule possesses two H atoms bonded to N3a; hence, H-bonds could possibly form with either the N1, N2, or N4 atom of the neighboring molecule. Calculations, however, reveal that the adsorption geometry is not suitable for such bonds to develop.

4.2.3. Organometallic Association of Deprotonated Molecules. Organic molecules may form self-assembled organometallic network structures on metal surfaces. For example, let us mention the structurally well characterized trimesic acid (TMA) on Cu(110), where TMA molecules are linked together by dimers of Cu adatoms.[66]

For benzotriazole, it has been frequently proposed that it forms a Cu(I)−BTA surface complex involving the Cu−N bonds,[9,10,18,67−80] but the actual structure and its bonding to the metal surface are still open issues. Determination of the exact surface structure is aggravated by the fact that it is different from the structure of the synthesized Cu(I)−BTA complex, which was shown to be amorphous.[9,26] It has been postulated that the surface complex forms a linear polymeric-like structure consisting of alternating Cu^+ and BTA^- ions in 1:1 ratio, forming a −Cu−BTA−Cu−BTA− bidentate structure.[9,18,74]

For this reason, several simple models of organometallic association of deprotonated molecules are considered below. We start with isolated complexes, where individual deprotonated molecules are linked to Cu ions. The following structures are considered: a simple Mol−Cu monomer, a Mol−Cu−Mol dimer, and a periodic $[MolCu]_n$ linear polymer structure (necklace). In the monomer and dimer, the Cu is bonded to a deprotonated molecular site, i.e., to the N1 atom for $ATA^{\odot}$ and $BTA^{\odot}$ and to the O1a atom for $BTAO^{\odot}$. The structures of $[MolCu]_n$ are derived from dimer structures. The resulting optimized structures are shown in Figure 9. All three inhibitors possess *unsaturated* atoms available for bonding with Cu, and their structures are such that the resulting intermolecular associations are not sterically hindered. Moreover, the structure of $ATA^{\odot}$ is also suitable for the formation of a two-dimensional planar-like organometallic network structure (see Figure 9).

Concerning the Mol−Cu bond strengths, the strongest bonds are formed with $BTA^{\odot}$, $D_{bond} \in [2.8,3.0]$ eV, followed by $ATA^{\odot}$, $D_{bond} \in [2.3,2.5]$ eV, whereas $BTAO^{\odot}$ forms the weakest bonds, $D_{bond} \in [1.8,2.1]$ eV. This trend is compatible with the molecule−surface bonding as measured by the $E^{\odot}_{ads}$ chemisorption energies (Figure 5). These results clearly show that dehydrogenated N atoms are able to form stronger bonds with Cu than dehydrogenated O atoms. Moreover, also the N−H

(64) Fang, B.-S.; Olson, C. G.; Lynch, D. W. *Surf. Sci.* **1986**, *176*, 476–490.
(65) Jiang, Y.; Adams, J. B. *Surf. Sci.* **2003**, *529*, 428–442.
(66) Classen, T.; Fratesi, G.; Costantini, G.; Fabris, S.; Stadler, F. L.; Kim, C.; de Gironcoli, S.; Baroni, S.; Kern, K. *Angew. Chem., Int. Ed.* **2005**, *44*, 6142–6145.
(67) Morito, N.; Suëtaka, W. *J. Jpn. Inst. Metals* **1971**, *35*, 1165–1170.
(68) Roberts, R. F. *J. Electron. Spectrosc.* **1974**, *4*, 273–291.
(69) Lewis, G.; Fox, P. G. *Corros. Sci.* **1978**, *18*, 645–650.
(70) Fox, P. G.; Lewis, G.; Boden, P. J. *Corros. Sci.* **1979**, *19*, 457–467.
(71) Chadwick, D.; Hashemi, T. *J. Electron. Spectrosc.* **1977**, *10*, 79–83.
(72) Chadwick, D.; Hashemi, T. *Corros. Sci.* **1978**, *18*, 39–51.
(73) Hashemi, T.; Hogarth, C. A. *Electrochim. Acta* **1988**, *33*, 1123–1127.
(74) Rubim, J. C.; Gutz, I. G. R.; Sala, O.; Orville-Thomas, W. J. *J. Mol. Struct. (Theochem)* **1983**, *100*, 571–583.
(75) Youda, R.; Nishihara, H.; Aramaki, K. *Corros. Sci.* **1988**, *28*, 87–96.
(76) Youda, R.; Nishihara, H.; Aramaki, K. *Electrochim. Acta* **1990**, *35*, 1011–1017.
(77) Brusic, V.; Frisch, M. A.; Eldridge, B. N.; Novak, F. P.; Kaufman, F. B.; Rush, B. M.; Frankel, G. S. *J. Electrochem. Soc.* **1991**, *138*, 2253–2259.
(78) Finšgar, M.; Kovač, J.; Milošev, I. *J. Electrochem. Soc.* **2010**, *157*, C52–C60.
(79) Biggin, M. E.; Gewirth, A. A. *J. Electrochem. Soc.* **2001**, *148*, C339–C347.
(80) Schultz, Z. D.; Biggin, M. E.; White, J. O.; Gewirth, A. A. *Anal. Chem.* **2004**, *76*, 604–609.

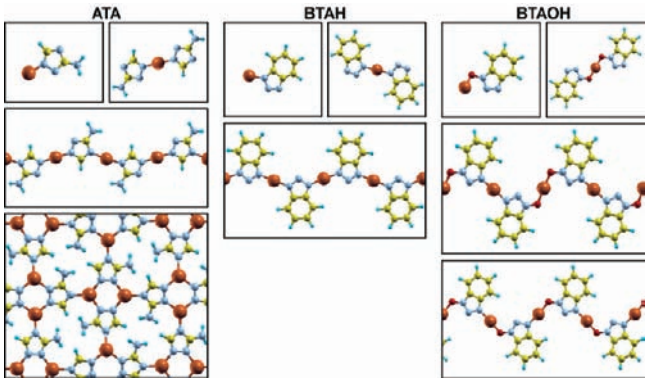

Figure 9. Optimized structures of organometallic complexes formed between Cu cation and deprotonated ATA, BTA, and BTAO anions. Monomer, dimer, and periodic linear polymer models are shown, and for ATA also a two-dimensional network structure. For [BTAO-Cu]$_n$ polymer, two energetically degenerate structures are shown: the bottom model is characterized by N−Cu−O organometallic bonding and the upper model by alternate N−Cu−N and O−Cu−O bonding.

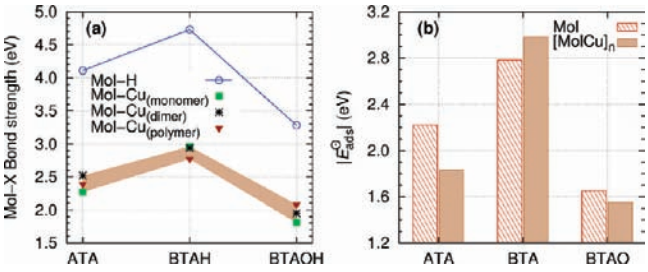

Figure 10. (a) Trend of Mol−H and Mol−Cu bond strenghts for ATA, BTAH, and BTAOH. As for the Mol−Cu, the bond energies of monomer, dimer, and polymer complexes are considered, and their span is shown by a brown band. (b) Stability of stand-alone deprotonated molecules (Mol) and organometallic necklaces ([MolCu]$_n$) adsorbed on Cu(111) as measured by the magnitude of $E^{\odot}_{ads}$.

bonds are stronger than the O−H bond in the parent neutral molecules. In particular, the D_{bond} values of the N−H bonds are calculated to be 4.73 and 4.11 eV for BTAH and ATA, respectively, whereas the D_{bond} of BTAOH's O−H bond is merely 3.28 eV. Hence, these N−H and O−H bond energies show the same trend as the Cu−N and Cu−O bonds. These trends are shown graphically in Figure 10a.

Organometallic Necklaces on Cu(111). The structure and energetics of [MolCu]$_n$ organometallic complexes on Cu(111) surfaces are considered next. Figure 11 shows the optimized structure of the [BTA−Cu]$_n$ organometallic necklace structure on Cu(111) at two different coverages. The stability of [BTA−Cu]$_n$ is almost independent of the coverage, and the organometallic necklaces can be densely packed, as shown in the middle panel of Figure 11. The bonding geometry of BTA

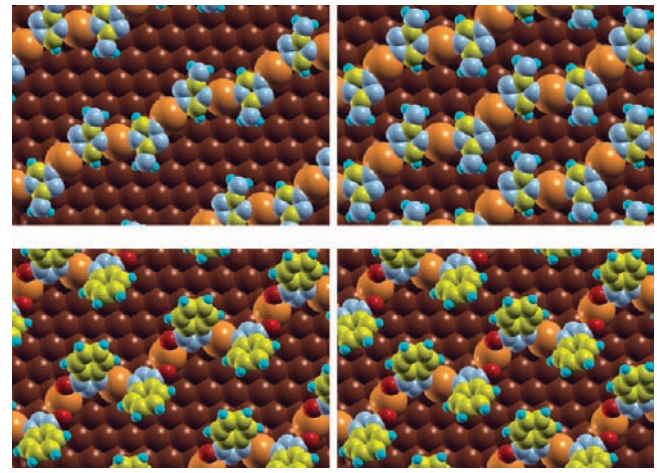

Figure 12. Snapshots of the optimized [ATA−Cu]$_n$ (top row) and [BTAO−Cu]$_n$ (bottom row) organometallic necklaces on Cu(111) at lower (left column) and higher (right column) coverage.

within the adsorbed organometallic necklace is shown in the right panel of Figure 11. It is evident that all the three N atoms of BTA are involved in bonding to Cu. The N1 and N3 atoms are bonded with Cu adatoms, thus constituting the necklace, whereas the N2 is bonded to the surface, in particular, to top and bridge sites. Analogous optimized structures of [ATA−Cu]$_n$ and [BTAO−Cu]$_n$ organometallic necklaces on Cu(111) are shown in Figure 12. The necklace formation energies, $E^{\odot}_{form}$, defined by eq S9 in the Supporting Information, are −1.83, −2.98, and −1.55 eV/molecule for [ATA−Cu]$_n$, [BTA−Cu]$_n$, and [BTAO−Cu]$_n$ on Cu(111), respectively. To establish whether the formation of necklaces is energetically preferred over the stand-alone adsorbed deprotonated molecules, the $E^{\odot}_{form}$ values of the former should be compared to $E^{\odot}_{ads}$ values of the latter, which are −2.22, −2.78, and −1.65 eV for ATA$^{\odot}$, BTA$^{\odot}$, and BTAO$^{\odot}$, respectively. The comparison therefore reveals that only the formation of the [BTA−Cu]$_n$ necklace is energetically favored, whereas for ATA and BTAO the adsorption of stand-alone deprotonated molecules is preferred instead. These relative stabilities are shown graphically in Figure 10b. Note, however, that the stability of organometallic necklaces on the surface is even larger than anticipated from the $E^{\odot}_{form}$ values, because their formation is activated. To illustrate the point, the formation energy of [BTA−Cu]$_n$ is −2.98 eV, but to remove a single BTA molecule from the necklace costs about 3.5 eV.

4.3. Adsorption-Induced Dipole Moment and Change of Work Function. To facilitate the understanding of the electric field effects on the molecule−surface bonding (presented in section 5.1), the gas-phase adsorption-induced dipole moments, μ, and work function changes, $\Delta\Phi$, in the absence of the external electric field are reported in Table 3. In the simple Helmholtz

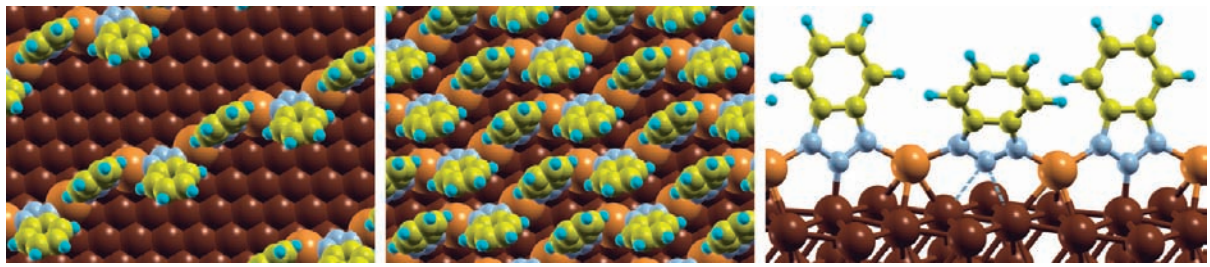

Figure 11. Snapshots of the optimized [BTA−Cu]$_n$ organometallic necklaces on Cu(111). Left and middle pictures show lower and higher densities of organometallic necklaces on the surface, respectively. Right picture shows the details of [BTA−Cu]$_n$ bonding to the surface.

Table 3. Molecular Löwdin Charges, $q_{\text{Löwdin}}$ (Positive Numbers Indicate Electron Excess), Adsorption-Induced Dipole Moments, μ, and Work Function Changes, $\Delta\Phi$

species	adsorption mode	Θ[a] (ML)	$q_{\text{Löwdin}}$ (electron)	μ (D)	$\Delta\Phi$ (eV)
		Chemisorption			
ATA	top-N2	1/16	−0.12	1.34	−0.54
BTAH	bridge-N2,N3	1/16	−0.03	4.77	−1.92
	top-N2	1/16	−0.12	3.81	−1.53
BTAOH	bridge-N2,N3	1/16	−0.05	3.98	−1.60
$ATA^{\odot}$	bridge-N1,N2	1/16	+0.52	−0.01	+0.003
$BTA^{\odot}$	bridge-N2,N3	1/16	+0.58	0.53	−0.22
	$[BTA-Cu]_n$	2/23	+0.59	1.91	−1.07
$BTAO^{\odot}$	bridge-O1a,N2	1/16	+0.60	1.23	−0.50
	bridge-N2,N3	1/16	+0.60	0.71	−0.29
$Cl^{\odot}$	fcc	1/9	+0.49	−0.33	+0.23
		Physisorption			
ATA	H-polymer	1/5	−0.07	0.88	−1.15
BTAH	stand-alone	1/16	−0.04	1.35	−0.55
	H-polymer	1/10	−0.02	1.10	−0.72
BTAOH	stand-alone	1/16	+0.07	0.11	−0.04

[a] Θ is the adsorbate coverage on Cu(111) in monolayers (ML).

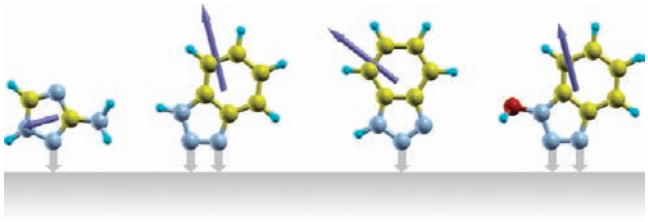

Figure 13. Dipoles moments of gas-phase ATA, BTAH, and BTAOH shown as dark blue arrows pointing from the barycenter of the molecules. The molecules are plotted in the orientation of their adsorbed state.

picture, the $\Delta\Phi$ is related to adsorption-induced dipole moment by $\Delta\Phi = -4\pi\theta\mu$ (in atomic units, where θ is the absolute coverage), where a positive value of μ stands for an outward-pointing dipole with the negative end at the surface and the positive end pointing outward (i.e., $\mu = \boldsymbol{\mu}\cdot\mathbf{n}$, where $\mathbf{n}$ is the surface normal).

The neutral molecules either in chemisorbed or in physisorbed state lower the surface work function, and in some cases the reduction is quite substantial, e.g., for BTAH and BTAOH in the bridge-N2,N3 chemisorbed state. To explain this effect, we plot in Figure 13 the molecules oriented as in the chemisorbed state with the gas-phase dipole moments shown as arrows. The calculated gas-phase dipole moments of ATA, BTAH, and BTAOH are 1.70, 4.07, and 3.54 D, respectively. In the absence of molecule−surface interaction, the dipole points outward and almost perpendicularly to the surface for BTAH and BTAOH in the bridge-N2,N3 geometry, whereas for ATA the dipole moment is almost parallel to the surface. The adsorption-induced dipole moments for bridge-N2,N3 BTAH and BTAOH are 4.77 and 3.98 D, hence being larger than the respective gas-phase values. This is due to the polarization induced by the molecule−surface interaction. According to Löwdin population analysis (Table 3), molecules donate a small amount of electron charge to the surface. This polarization also explains why the work function lowers for chemisorbed ATA and for the physisorbed molecules.

The adsorption-induced dipole moments are much smaller for deprotonated molecules. Note that, in this case, the adsorbed molecules are partially charged by about half an electron (see Löwdin charges in Table 3), and this counteracts the effect of the molecular dipole. Nevertheless, the adsorption-induced dipole moments are still positive, thus resulting in the negative work function changes, except for the deprotonated ATA, for which the adsorption-induced dipole is vanishing.

Table 4. Constituent Energy Contributions and the Resulting Adsorption Free Energies at the Cu(111)/Water Interface for Neutral Molecules

species	adsorption mode	E_{ads} (eV)	$\Delta G_{\text{solv}}^{\text{MolH}}$ (eV)	$\Delta\Delta G_{\text{solv}}^{\text{MolH//Cu}}$ (eV)	$\Delta G_{\text{ads}}^{(\text{aq})}$ (eV)
		Chemisorption			
ATA	top-N2	−0.60	−0.55	0.02	−0.03
BTAH	top-N2	−0.40	−0.41	0.05	0.06
	bridge-N2,N3	−0.37	−0.41	0.11	0.15
BTAOH	bridge-N2,N3	−0.53	−0.44	0.29	0.20
		Physisorption			
ATA	H-polymer	−1.12	−0.55	0.34	−0.23
BTAH	stand-alone	−0.74	−0.41	−0.03	−0.36
	H-polymer	−1.23	−0.41	0.35	−0.47
BTAOH	stand-alone	−0.97	−0.44	0.16	−0.37

5. Adsorption at Metal/Water Interface

Adsorption at the metal/water interface is modeled with the method described in section 2.1 and in more detail in section S2.2 in the Supporting Information. While the gas-phase adsorption energy can be used as a measure of the molecule−surface bond strength, the energy of adsorption from the aqueous phase is a result of several competing effects: molecule−water, molecule−metal, metal−water, and the water−water interactions. It is therefore reasonable to expect the adsorption energies at the metal/water interface to be less exothermic compared to the gas-phase adsorption energies.

As for the neutral species, the expression for free energies of adsorption consists of three terms, $\Delta G_{\text{ads}}^{(\text{aq})} = E_{\text{ads}} - \Delta G_{\text{solv}}^{\text{MolH}} + \Delta\Delta G_{\text{solv}}^{\text{MolH//Cu}}$, which are reported in Table 4 together with the resulting adsorption free energies. As evident from the table, the molecular solvation free energies, $\Delta G_{\text{solv}}^{\text{MolH}}$, are about −0.4 to −0.5 eV, thus being similar to gas-phase adsorption energies. The two terms therefore largely cancel each other out, while the $\Delta\Delta G_{\text{solv}}^{\text{MolH//Cu}}$ contribution is slightly endothermic, up to 0.3 eV. All these result in $\Delta G_{\text{ads}}^{(\text{aq})}$ values that are less exothermic than the gas-phase adsorption energies.

It is further evident from Table 4 that the stabilization effect due to intermolecular H-bonding between inhibitor molecules on the surface is much reduced in the aqueous phase with respect to the gas phase; compare, for example, the E_{ads} and $\Delta G_{\text{ads}}^{(\text{aq})}$ values for stand-alone physisorbed BTAH to those of physisorbed H-bonded polymer of BTAH. While in the gas phase the stabilization due to intermolecular H-bonding is about 0.5 eV/molecule, it is reduced to 0.1 eV/molecule in the aqueous phase. The reason is that, in the aqueous phase, the stand-alone physisorbed inhibitor molecules form H-bonds with water molecules, yet these H-bonds are not as strong as the inhibitor−inhibitor H-bonds; e.g., the bond strength of a single H-bond between BTAH and H_2O is 0.37 eV, whereas that within a BTAH polymer is 0.52 eV.

As for the deprotonated species or anions, the expression for free energy of adsorption, eq 5, consists of five terms: the three present already for neutral species plus two additional, which are the electron affinity of the molecular radical, $E_{\text{ea}}^{\odot}$, and the metal/water/vacuum work function, Φ^*. These terms are reported in Table 5, together with the resulting adsorption free energies. For comparison purposes, also the values for the Cl^- anion are reported. In contrast with the neutral species, all the terms but the $\Delta\Delta G_{\text{solv}}^{\text{Mol//Cu}}$ are large in magnitude. However, there

Table 5. Constituent Energy Contributions and the Resulting Adsorption Free Energies at Cu(111)/Water Interface for Deprotonated Molecules

	adsorption mode	$E^{\odot}_{ads}$ (eV)	$\Delta G^{Mol^-}_{solv}$ (eV)	Δ	$E_{ea}{}^{\odot}$ (eV)	Φ^* (eV)	Δ	$\Delta\Delta G^{Mol H//Cu}_{solv}$ (eV)	$\Delta G^{(aq)}_{ads}$ (eV)
ATA^-	bridge-N1,N2	−2.22	−2.78	(= 0.56)	2.39	3.95	(= −1.56)	−0.11	−1.11
BTA^-	$[BTA-Cu]_n$	−2.98	−2.39	(= −0.59)	3.53	3.95	(= −0.42)	−0.07[a]	−1.08
	bridge-N2,N3	−2.78	−2.39	(= −0.39)	3.53	3.95	(= −0.42)	−0.07	−0.88
$BTAO^-$	bridge-O1a,N2	−1.65	−2.36	(= 0.71)	2.58	3.95	(= −1.37)	−0.12	−0.78
	bridge-N2,N3	−1.58	−2.36	(= 0.78)	2.58	3.95	(= −1.37)	−0.10	−0.69
Cl^-	fcc	−3.31	−3.06	(= −0.25)	3.69	3.95	(= −0.26)	−0.09	−0.60

[a] Approximated by the value of the bridge-N2,N3 form.

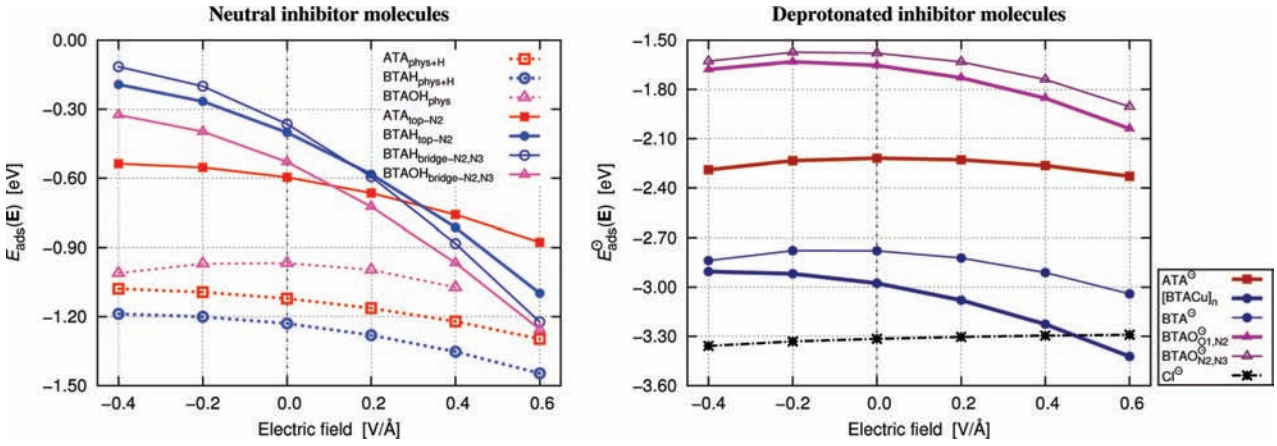

Figure 14. Adsorption energy of neutral (left) and dehydrogenated (right) inhibitors as a function of electric field, $E_{ads}(\mathbf{E})$ and $E^{\odot}_{ads}(\mathbf{E})$, respectively. For comparison, the data for $Cl^{\odot}$ are also presented on the right plot. In the legend, the subscript "phys+H" stands for the physisorbed H-bonded polymers (cf. Figure 8), and the subscript "phys" stands for the stand-alone physisorbed molecule.

is a very large mutual cancellation of the terms, resulting in the moderate $\Delta G^{(aq)}_{ads}$. In particular, the anion solvation energies, $\Delta G^{Mol^-}_{solv}$, are highly exothermic, but so are the molecule−surface bond strengths, as measured by $E^{\odot}_{ads}$. Also the competition for the electron between being in the anion or the metal, $E^{\odot}_{ea} - \Phi^*$, results in moderate cancellation. The resulting $\Delta G^{(aq)}_{ads}$ values range from −1.1 to −0.6 eV, which are substantially smaller in magnitude compared to the gas-phase analogues. Moreover, due to this effective cancelation between the various terms, the preference for the adsorption of deprotonated molecules over the adsorption of neutral molecules is substantially reduced in the aqueous phase compared to the gas phase.

It is interesting to notice that, while the Cl−surface bond is stronger than the inhibitor−surface bonds, as measured by $E^{\odot}_{ads}$, Cl^- also displays more exothermic solvation and larger $Cl^{\odot}$ electron affinity. For these reasons, Cl^- exhibits the least exothermic value of $\Delta G^{(aq)}_{ads}$ in Table 5. Qualitatively this means that the bonding of inhibitors to the surface is more competitive with the bonding of Cl^- at the metal/water interface than at the metal/vacuum interface. Moreover, the magnitudes of the $\Delta G^{(aq)}_{ads}$ follow the trend $ATA^- \approx BTA^- > BTAO^-$, indicating that ATA^- and BTA^- would compete more efficiently with Cl^- for the adsorption sites than $BTAO^-$. Although this suggests a plausible explanation of the experimental determined inhibition performance of the three corrosion inhibitors, the double-layer electric field effects on the molecule−surface bonding should be addressed before making any definite claims.

5.1. Electric Field Effects in the Double Layer. The electric field (or the applied electrode potential) influences the adsorption free energy due to several effects, which according to the current model can be decomposed into (i) variation of the molecule−surface bonding, (ii) variation of contribution due to electron transfer from anion to electrode (or to cation from electrode), and (iii) variation of the $\Delta\Delta G^{Mol//Cu}_{solv}$ term.

The effect of the applied electric field on the molecule−surface bonding can be anticipated from the adsorption-induced dipole moment. If the adsorption-induced dipole moment is aligned with the applied electric field, an enhancement of molecule−surface bonding can be expected, and vice versa for the anti-oriented dipole. Because in the current case the adsorption-induced dipole moments are positive (Table 3), an enhancement of the molecule−surface bonding can be anticipated with increasing the electric field **E** in the positive direction (i.e., for small fields $E_{ads}(\mathbf{E}) - E_{ads}(0) \approx -\boldsymbol{\mu}\cdot\mathbf{E}$). This is indeed the case, as can be seen from Figure 14, which plots the E_{ads} as a function of electric field. All the chemisorbed neutral species display a negative slope of $E_{ads}(\mathbf{E})$ in the range considered. The steepest negative slope is displayed by chemisorbed BTAH, followed by BTAOH, as would be anticipated on the basis of the adsorption-induced dipole moments (Table 3). For chemisorbed ATA and all the physisorbed molecules, the dependence on **E** is more gradual. Also, deprotonated species display less pronounced $E^{\odot}_{ads}$ dependence on **E**, and for deprotonated ATA the curve is very flat and symmetric around $|\mathbf{E}| = 0$, in accord with its vanishing adsorption-induced dipole moment (Table 3). Figure 14 also plots the $E^{\odot}_{ads}$ dependence on **E** for chlorine, which is almost linear, with a small positive slope, in accord with its negative (and small in magnitude) adsorption-induced dipole moment of −0.3 D.[81]

For deprotonated species or anions, also a contribution from electron transfer to the electrode, $-\Phi^*(\mathbf{E})$, should be considered [i.e., $E^{\ominus}_{ads}(\mathbf{E}) = E^{\odot}_{ads}(\mathbf{E}) + E^{\odot}_{ea} - \Phi^*(\mathbf{E})$]. In the Helmholtz−Perrin double-layer model, this contribution decreases linearly with increasing electric field, and the slope of the $\Phi^*(\mathbf{E})$ is given by

(81) The value of the Cl adsorption-induced dipole moment of −0.3 D is taken from ref 45. Note that, in ref 45, the opposite sign convention is used for the dipole moment.

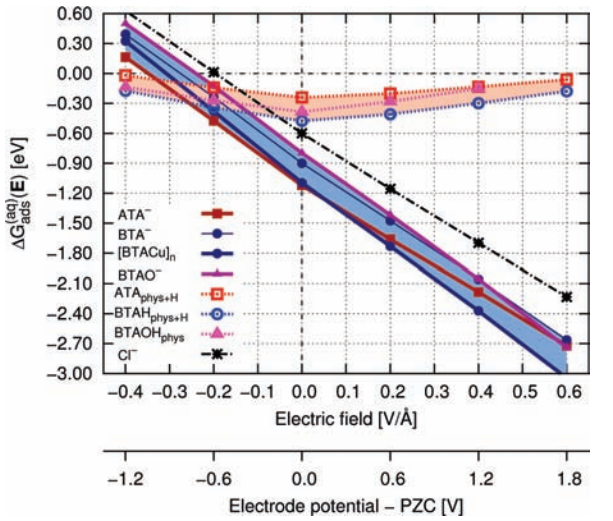

Figure 15. Adsorption free energies, $\Delta G^{(aq)}_{ads}(\mathbf{E})$, for neutral (light red band) and deprotonated (light blue band) inhibitors as a function of electric field (electrode potential). The data for Cl^- are also presented (black dot-dashed line). The link between the electric field and the electrode potential (relative to static PZC) is made by setting the thickness of the double layer to $d = 3$ Å (cf. eq 7). Were a larger value used for d, the slope of the $\Delta G^{\ominus(aq)}_{ads}$ vs **E** (light blue band and black dot-dashed line) would be steeper, and vice versa for a smaller value of d.

the thickness of the double layer, eq 7, which as specified in section 2.1 is set to 3 Å for illustrative purposes. On this basis, we present in Figure 15 the dependence of the $\Delta G^{(aq)}_{ads}$ on the applied electric field. To enhance the readability of Figure 15, the energy range spanned by neutral molecules is designated by the light red band, and that of deprotonated molecules is designated by the light blue band. In this figure, the electrode potential relative to the potential of zero charge (PZC) is also indicated with the aid of eq 7. Because the current PZC corresponds to a static potential of zero charge, which can be different from the measurable potential of zero charge,[82] and because of the postulated thickness of the double layer ($d = 3$ Å), the indicated electrode potential should be taken merely as an approximate guide.

As for the neutral molecules, the $\Delta G^{(aq)}_{ads}(\mathbf{E})$ values display the well-known *parabolic* dependence for organic molecules, with the strongest adsorption at the PZC.[83] On the other hand, for deprotonated molecules, the exothermicity of the $\Delta G^{(aq)}_{ads}(\mathbf{E})$ values monotonically and steeply increases with electrode potential, which is due to the $-\Phi^*(\mathbf{E}) = -ed\mathbf{nE}$ term. The adsorption of neutral molecules is therefore competitive with deprotonated forms only at low electrode potentials, whereas at higher electrode potentials deprotonated forms become substantially more stable than the neutral forms. This behavior is strongly supported by experiments[28,75,84,85] and suggests that deprotonated forms are the active species for inhibiting the corrosion. This proposition is further corroborated by evidence that benzotriazole is less efficient in acidic solutions,[86−89] where the amount of deprotonated species is decimated, and moreover by the fact that 1-methylbenzotriazole is ineffective in preventing Cu corrosion,[90] because the substitution of H1a by a methyl group prevents the formation of BTA^-.

It can be further ascertained from Figure 15 that, among the three deprotonated inhibitors, $BTAO^-$ is the least stable over the whole investigated range, which is compatible with the experimental observation that, upon the addition of BTAH into BTAOH-containing solution, the BTAOH is replaced by BTAH on the surface.[27] The stabilities of BTA^- in $[BTA{-}Cu]_n$ form and ATA^- are comparable at potentials around static PZC (i.e., zero applied electric field). At negative applied electric field, the ATA^- is slightly more stable than $[BTA{-}Cu]_n$; however, the range of its *superiority* is limited, because at sufficiently negative potential, the neutral forms become the most stable. The opposite is true for potentials more positive than the static PZC, where the $[BTA{-}Cu]_n$ is the stablest, and its relative stability compared to others increases with electrode potential, in good agreement with experimental findings.[76,91] Note, however, that in the range of applied electric field from −0.2 to +0.2 V/Å, the difference in stability between $[BTA{-}Cu]_n$ and ATA^- is not significant and certainly below the estimated accuracy, in particular due to all the approximations used in obtaining the $\Delta G^{(aq)}_{ads}(\mathbf{E})$ values. On this basis, it can be concluded that the order of adsorption stability is $BTA^- \approx ATA^- > BTAO^-$, which is consistent with the trend of experimentally determined corrosion inhibition performance. A factor that may contribute to somewhat inferior inhibition performance of ATA compared to BTAH may be its high pK_a value, because only a tiny fraction of ATA is in the active deprotonated form at near-neutral pH conditions. This is consistent with the observation that, under more alkaline conditions (pH = 9), where the amount of the deprotonated form is larger, ATA outperforms BTAH in some aspects of corrosion (i.e., pitting corrosion).[19]

All three deprotonated inhibitor molecules display more exothermic adsorption than the Cl^- anion, irrespective of the electrode potential. It must be pointed out that, due to approximations used in the evaluation of adsorption free energies at the electrified surface, the comparison among molecules of similar size is more reliable as a result of error cancelation. The comparison among the inhibitor molecules is therefore more reliable than comparison of inhibitors to the Cl^- anion. Nevertheless, even if the energy magnitudes for Cl^- are underestimated by 0.5 eV with respect to those of inhibitors, the adsorption of ATA^- and BTA^- would still be preferred to that of Cl^-, in agreement with experiments according to which the BTAH excludes the Cl^- from the surface whereas the BTAOH is coadsorbed with Cl^-.[27]

(82) Taylor, C. D.; Wasileski, S. A.; Filhol, J.-S.; Neurock, M. *Phys. Rev. B* **2006**, *73*, 165402.
(83) Bockris, J. O.; Reddy, A. K. N.; Gamboa-Aldeco, M. *Modern Electrochemistry*, 2nd ed.; Kluwer Academic/Plenum Publishers: New York/Boston/Dordrecht/London/Moscow, 2000; Vol. 2A.
(84) Hope, G. A.; Schweinsberg, D. P.; Fredericks, P. M. *Spectrochim. Acta Part A: Mol. Spectrosc.* **1994**, *50*, 2019–2026.
(85) Chan, H. Y. H.; Weaver, M. J. *Langmuir* **1999**, *15*, 3348–3355.
(86) Musiani, M.; Mengoli, G.; Fleischmann, M.; Lowry, R. *J. Electroanal. Chem.* **1987**, *217*, 187–202.
(87) Al-Kharafi, F. M.; Ateya, B. G. *J. Electrochem. Soc.* **2002**, *149*, B206–B210.
(88) Brunoro, G.; Parmigiani, F.; Perboni, G.; Rocchini, G.; Trabanelli, G. *Br. Corros. J.* **1992**, *27*, 75–79.
(89) Tommesani, L.; Brunoro, G.; Frignani, A.; Monticelli, C.; Colle, M. D. *Corros. Sci.* **1997**, *39*, 1221–1237.
(90) Törnkvist, C.; Thierry, D.; Bergman, J.; Liedberg, B.; Leygraf, C. *J. Electrochem. Soc.* **1989**, *136*, 58–64.
(91) Morito, N.; Suëtaka, W. *J. Jpn. Inst. Metals* **1973**, *37*, 216–221.
(92) Weaver, M. J. *Appl. Surf. Sci.* **1993**, *67*, 147–159.
(93) Koper, M. T. M.; van Santen, R. A.; Wasileski, S. A.; Weaver, M. J. *J. Chem. Phys.* **2000**, *113*, 4392–4407.
(94) Wasileski, S. A.; Koper, M. T. M.; Weaver, M. J. *J. Phys. Chem. B* **2001**, *105*, 3518–3530.
(95) Schultze, J. W.; Rolle, D. *J. Electroanal. Chem.* **2003**, *552*, 163–169.

All these findings therefore corroborate the competitive adsorption scenario as a plausible mechanism for inhibiting the corrosion of copper in near-neutral chloride solutions.

6. Conclusion

Corrosion inhibition performance of three corrosion inhibitors for copper — ATA, BTAH, and BTAOH — in near-neutral chloride solution was investigated by corrosion experiments and atomistic computer simulations. The trend of inhibition performance was determined experimentally as BTAH $\gtrsim$ ATA $\gg$ BTAOH. To disentangle the factors involved in the inhibition of corrosion with the aid of extensive computer simulations based on density functional theory, an approximate scheme to treat the adsorption at an electrified surface was introduced. Grasping the factors involved in the corrosion inhibition mechanism was possible only by means of a careful analysis of several phenomena: (i) interaction of neutral and deprotonated inhibitor molecules with the surface, (ii) role of intermolecular association of inhibitors on the surface, (iii) solvation effects, (iv) double-layer electric field effects on the molecule−surface bonding, and (v) comparison of inhibitors−surface bonding to that of aggressive chloride anions.

Our findings affirm the competitive adsorption scenario as a plausible mechanism for inhibiting the corrosion of copper in near-neutral chloride solutions. The superior corrosion inhibition performance of BTAH and ATA is attributed to their ability to form strong N−Cu chemical bonds in the deprotonated form and to the interplay of competing solvation effects. These N−Cu bonds are not as strong as the Cl−Cu bonds, yet the presence of solvent favors the adsorption of inhibitor molecules onto the surface due to a stronger solvation of the Cl^- anions. Moreover, benzotriazole displays the largest affinity among the three corrosion inhibitors to form intermolecular organometallic aggregates, e.g., $[BTA-Cu]_n$ polymeric complex, which is another factor contributing to its outstanding corrosion inhibition performance. Not only do such organometallic complexes contribute to an increased stability of the protective benzotriazole film on the surface, but they also allow for a very dense and effective packing of the inhibitor on the surface, thus making the inhibitor surface film an effective barrier against diffusion of aggressive ions from solution to the copper surface.

The inhibition of corrosion is a complex phenomenon due to an interplay of several effects. The outcome of the interplay depends on various conditions, such as the pH, electrode potential, the chemical and physical nature of the metal in question, and the presence of reactive species in solution. Hence, a particular corrosion inhibitor works well under given circumstances and not necessarily for others. In this respect, it is not surprising that the current trend of corrosion inhibition performance cannot be anticipated, neither on the basis of the inhibitor's molecular electronic structure alone[24] — an approach that is proliferating in the literature[4] — nor on the basis of gas-phase adsorption calculations. This emphasizes the importance of a rigorous modeling of the interactions between the components of the corrosion system in the corrosion inhibitor studies employing quantum chemical calculations.

Acknowledgment. This work has been supported by the Slovenian Research Agency (Grants Nos. J1-9516, J1-2240, and P2-0148).

Supporting Information Available: Complete refs 32 and 35; experimental and computational details, including the method introduced to model the adsorption at the electrified surfaces. This material is available free of charge via the Internet at http://pubs.acs.org.

JA107704Y